ChemPubSoc Europe

DOI: 10.1002/cssc.201403464

CHEMSUSCHEM Full Papers

Synthesis and Nanostructures of Metal Selenide Precursors for Cu(In,Ga)Se_2 Thin-Film Solar Cells

Ji-Hyun Cha, Se Jin Noh, and Duk-Young Jung*[a]

A nanoink solution-based process was developed as a low-costing method for the fabrication of Cu(In,Ga)Se_2 (CIGSe) thin-film photovoltaic cells. The sonochemical synthesis of CIGSe nanocrystals of the nanoink through step-by-step mixing of the reactants was investigated. To achieve the ideal stoichiometry of Cu($In_{0.7}Ga_{0.3}$)Se_2 to tune the bandgap and to fabricate high-efficiency photovoltaic cells, the synthetic parameters, the concentration of hydrazine, and the amount used of the gallium precursor were investigated. As the hydrazine concentration increased, gallium loss was observed in the CIGSe product. The gallium content in the reactant mixture strongly affected the metal stoichiometry of the prepared CIGSe nanocrystals. The nanoink solution based fabrication of thin-film photovoltaic cells was also explored, and the resulting device showed a conversion efficiency of 5.17%.

Introduction

The development of low-costing and high-efficiency thin-film photovoltaic cells with semiconducting inorganic compounds is a major challenge to commercialize renewable and clean energy. Nanoparticles of Cu(In_xGa_{1-x})Se_2 (CIGSe) and related chalcogenide compounds have been proposed as promising materials for colloidal solution based syntheses for the large-scale fabrication of devices with efficiencies as high as 13.6%.[1–3] Recently, several colloidal solution approaches of CIGSe[4–9] and Cu-In-Ga[10–12] metals have been demonstrated for the fabrication of CIGSe thin-film solar cells. Important issues of the CIGSe colloidal solution are the control of the chemical compositions for band gap tuning, removal of surfactants from the precursor materials for high-quality absorber layers, and scale up of the CIGSe product. The indium-to-gallium ratio in the prepared CIGSe nanoparticles should be close to 2:1 to maintain the Cu($In_{0.7}Ga_{0.3}$)Se_2 composition for optimized bandgap energy and high light conversion efficiency.[13,14] Nanoparticles as precursors for thin films are generally synthesized by using long-chain organic surfactants, which leads to degradation of device performance. To fabricate high-efficiency photovoltaic (PV) cells, the surfactants of nanoparticles should be removed or replaced with inorganic ligands. In this respect, sonochemical synthesis solves these problems and provides a method to prepare large-scale, high-purity, surfactant-free CIGSe nanoparticles with a controlled chemical composition of Cu($In_{0.7}Ga_{0.3}$)Se_2.[15]

Transition-metal salts react with selenium in polar solvents by using metal precursors such as copper chloride, gallium nitrate, and indium acetate. The source of selenium is elemental selenium, which is partially reduced to selenide in solution through reaction with an alkylamine or hydrazine.[16] The first step involves rapid formation of the InSe phase through the reaction of indium acetate with selenium in a hydrazine/ethylene glycol/water medium, which is then followed by incorporation of gallium and copper to produce the final CIGSe. Critical parameters that affect particle size and chemical composition of the product include the mixing procedure, injection speed, reaction temperature, and time. For instance, one-pot mixing of the metal precursors, selenium, and bases (amines or hydrazine) produces unexpected side products that cannot be separated from the desired CIGSe nanoparticles. The prepared CIGSe nanoparticles for nanoinks should have precise stoichiometry of the four components (i.e., Cu, In, Ga, and Se), but partial dissolution of any component easily disturbs the successful synthesis of Cu($In_{0.7}Ga_{0.3}$)Se_2. In addition, CIGSe nanocrystals without capping agents have a reactive surface that is exposed to solvent molecules in the nanoink, and this results in their decomposition.

Although the syntheses of metal selenide compounds typically result in spontaneous reactions owing to the formation of a large amount of energy, the formation of thermodynamically stable binary selenide compounds, such as $Cu_{1-x}Se$, should be avoided during the syntheses of CIGSe nanoparticles.[17] To reveal the reaction mechanism involved in the synthesis of CIGSe nanoparticles, X-ray fluorescence spectroscopy (XRF) of the chemical compositions of the intermediates and evolution of their crystal structures by XRD measurements during the sonochemical syntheses are required. Quantitative analysis of the metal stoichiometry and the evolution of the crystal structures

[a] J.-H. Cha, S. J. Noh, Prof. D.-Y. Jung
Department of Chemistry, Center for Human Interface Nanotechnology
Sungkyunkwan Advanced Institute of Nanotechnology
Sungkyunkwan University
Suwon 440-746 (Republic of Korea)
E-mail: dyjung@skku.edu

Supporting Information for this article is available on the WWW under http://dx.doi.org/10.1002/cssc.201403464.

This publication is part of a Special Issue on "Sustainable Chemistry at Sungkyunkwan University". To view the complete issue, visit: http://onlinelibrary.wiley.com/doi/10.1002/cssc.v8.14/issuetoc.

of the precursors are important to determine the successful fabrication process of the CIGSe thin-film PV cells.

Herein, we present a systematic study of the step-by-step sonochemical reactions of the metal precursors of $Cu(In_{0.7}Ga_{0.3})Se_2$ nanoparticles under ambient conditions. Incorporation of the metal in each synthetic step of the synthesis was critical, as all of the precursors and reactants had low solubility in the alcohol-based reaction media. Changing the order of addition of the metal resulted in different crystal structures, and XRD simulations confirmed the chalcopyrite crystal structure of the prepared CIGSe nanoparticles. We also demonstrate the preparation of CIGSe nanoink, CIGSe thin films, and PV cells.

Results and Discussion

A CIGSe nanocrystal was synthesized by using a sonochemical method with Se powder, CuCl, indium acetate, and gallium nitrate in a mixture of hydrazine hydrate and ethylene glycol as the reaction medium (Figure 1). Elemental selenium was dispersed and partly dissolved in a 12.5% hydrazine/ethylene glycol solution to produce a dark brown color; this prevented oxidation of SeO_2 in the atmosphere.[16] Indium acetate was added to the selenium/hydrazine solution, and the resulting solution was treated by ultrasound at 110 °C; the dark brown solution slowly changed into a turbid colloidal solution with a yellow precipitate. The yellow In-Se powder was separated by centrifugation and showed a chemical composition of $In_{1.00}Se_{1.86}$, as measured by quantitative XRF analysis. Gallium nitrate was added to the In-Se colloidal solution, and this was followed by ultrasonic treatment, which produced a yellow solid precipitate with gallium inclusions, $(In_{0.68}Ga_{0.32})Se_{1.81}$. If gallium nitrate was added first to the selenium/hydrazine solution followed by the addition of indium acetate, the same In-Ga-Se precipitate was obtained. Gallium nitrate was completely dissolved in the selenium/hydrazine solution, and the addition of indium acetate caused In-Ga-Se to precipitate from the solution. The formation of In-Se drove the coprecipitation of In-Ga-Se, regardless of the sequence of addition of the two metal precursors in the selenium/hydrazine solution.

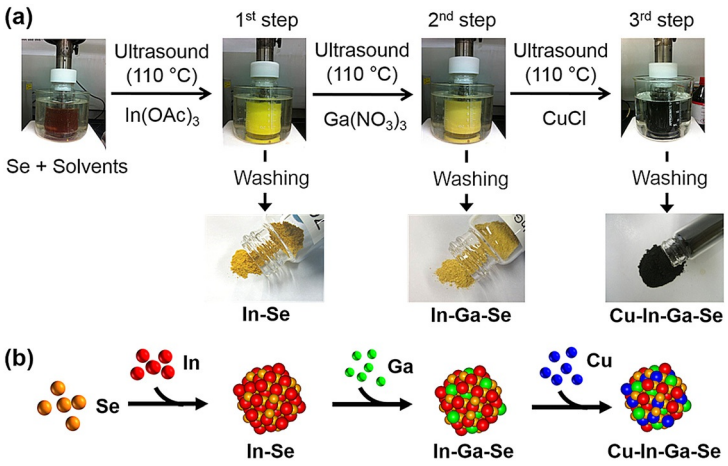

Figure 1. (a) Photographs of the synthesis process by using the sonochemical method and (b) schematic illustration of the formation of CIGSe nanoparticles.

The addition of copper chloride to the In-Ga-Se precursor under ultrasound quickly changed the precipitate color to deep black, and the composition of this material was confirmed to be $Cu_{1.00}(In_{0.68}Ga_{0.30})Se_{2.01}$ without any detectable quantity of any other metal by XRF. After annealing at 500 °C under an Ar atmosphere for 60 min, the chemical composition of CIGSe was $Cu_{1.0}(In_{0.71}Ga_{0.29})Se_{2.0}$. After the sonochemical synthesis, CIGSe particles precipitated from a clear colorless supernatant, which was evidence of the complete consumption of selenium. If all of the metal precursors are mixed at the same time in the selenide/hydrazine solution, the reaction time should be much longer than the subsequent mixing to avoid the formation of binary Cu-Se compounds. The copper precursor should be added after the other metals, because the various Cu-Se phases are very stable and nanocrystal growth is preferred.

The concentration of hydrazine (0 to 100%) in solution influenced the phase formation of CIGSe, as shown in the XRD analyses in Figure 2 (see also Figure S1, Supporting Information) and the metal compositions [Ga/(In+Ga)] estimated by XRF analyses. If hydrazine was not added to ethylene glycol, selenium did not dissolve, and only CuSe and Se were formed (Figure S1). A Lewis base, such as hydrazine or an alkylamine, is a prerequisite for the synthesis of CIGSe, because the amine groups stabilize the metal cations through the ligand and accommodate the formation of metal selenides.[17] Broad XRD peaks of the cubic structure were obtained for the as-prepared CIGSe samples, which is indicative of random arrangement of the metals in the CIGSe nanoparticles.

The CIGSe samples after annealing at 500 °C demonstrated compositional and structural variation as a function of the hydrazine concentration (Figure 3). Low concentrations of hydrazine, that is, 5.0 and 12.5%, resulted in small *c* axis values and a large Ga/

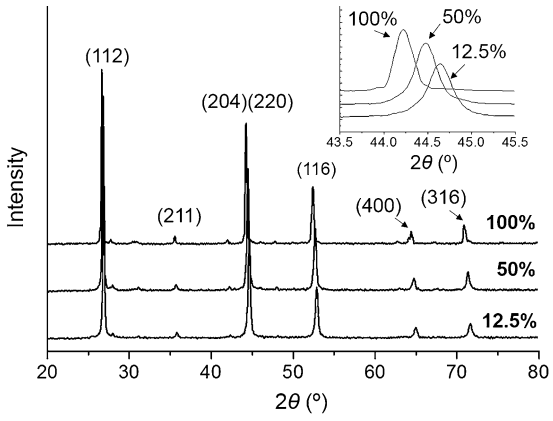

Figure 2. XRD spectra of sintered CIGSe nanoparticles prepared by sonochemical synthesis at different hydrazine concentrations. The inset shows the magnification of the (220)(204) XRD peaks of the CIGSe compounds.

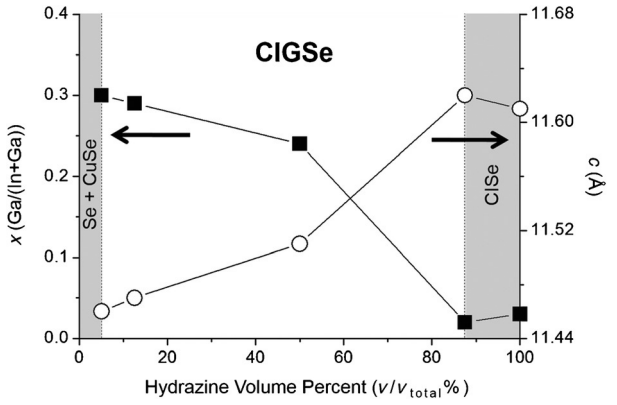

Figure 3. Variation of the lattice parameter *c* and the Ga(In + Ga) ratio as a function of hydrazine volume percent in the reaction media.

(In+Ga) ratio that approached the ideal Ga/(In+Ga) ratio of 0.30. A hydrazine concentration of 50% reduced the gallium content in CIGSe to 0.24 and resulted in an increase in both the *a* and *c* axes of the tetragonal unit cell owing to the high indium content. A neat hydrazine hydrate solution produced $Cu_{1.0}(In_{0.97}Ga_{0.03})Se_{2.0}$, which has only a small amount of gallium with a much larger cell volume than the 12.5% sample.

The concentration of the base was fixed at 12.5% to obtain the optimized metal ratio of CIGSe. Four CIGSe samples were synthesized and annealed at 500 °C; the weight of the gallium salt starting material ranged from 0.30 to 1.00 in Ga/(In+Ga) (denoted as *x*) and the hydrazine concentration was 12.5%. As the gallium content was increased, both axes of the tetragonal unit cell decreased linearly but in different proportions, as summarized in Table 1.[7] If the hydrazine concentration was increased in the reaction solvent, slightly Cu-rich CIGSe nanoparticles were obtained with a Cu/(In+Ga) ratio of approximately 1.04. Alternatively, increasing the Ga concentration of the reaction mixture resulted in In/Ga-rich nanoparticles.

If the gallium content was greater than $x = 0.5$ in the precursors, the synthesized CIGSe nanoparticles contained the $Cu_{2-x}Se$ phase, as observed in the XRD pattern, and this is detrimental for PV cell performance. The Raman spectra of the CIGSe samples confirmed the chalcopyrite crystal structure and the monotonous blueshift in the characteristic A_1 mode band as the gallium content was increased (Figure S2). If all the force constants were assumed to be equal, the band shift was a function of the reduced mass in the quaternary compounds according to Hook's law.[18] The calculated A_1 mode frequencies fit well with the experimental data, which were also in good agreement with the chemical composition estimated by XRF. The reflectance UV/Vis spectra provided the bandgap energy values through Kublka–Munk fitting, which indicated reliable tuning from 1.04 to 1.60 eV as the gallium content was increased (Figure S3).

The XRD data of $In_{1.00}Se_{1.86}$ (In-Se) in Figure 4 show the cubic structure with a lattice parameter of $a = 5.755(5)$ Å along with peaks for elemental selenium (JCPDF 27-0602), presumably because the stoichiometry of the starting materials was considered for the final CIGSe compound. $In_{1.00}Se_{1.86}$ was suggested to be a mixture of cubic $In_{1.00}Se_{1.00}$ and unreacted selenium residue. The poor solubility of selenium strongly influenced the crystal structures of InSe, that is, hexagonal and cubic struc-

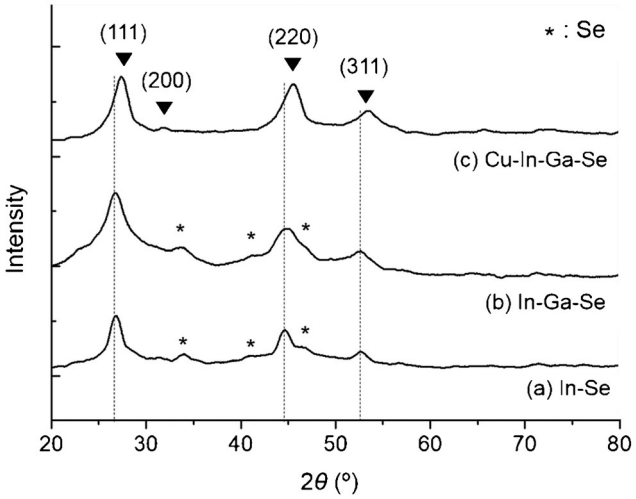

Figure 4. XRD patterns of (a) In-Se (1st step), (b) In-Ga-Se (2nd step), and (c) Cu-In-Ga-Se (3rd step).

Table 1. Chemical compositions and lattice parameters of the products obtained by variation of the hydrazine concentration and gallium content.

Experiment	Precursor	Hydrazine concentration [v/v_{total} %]	Product	Lattice parameters[a] [Å]		x[=Ga/(In + Ga)] vs. lattice parameters
				a	*c*	
hydrazine concentration	1.0 Cu + (0.7 In + 0.3 Ga) + 2.0 Se	0	$Cu_2Se + Se$	–	–	
		5.0	$Cu_{1.0}(In_{0.70}Ga_{0.30})Se_{2.0}$	5.73(3)	11.46(3)	
		12.5	$Cu_{1.0}(In_{0.71}Ga_{0.29})Se_{2.0}$	5.73(4)	11.47(4)	$a = 5.78 - 0.18x$
		50.0	$Cu_{1.0}(In_{0.66}Ga_{0.24})Se_{2.0}$	5.75(4)	11.51(4)	$c = 11.63 - 0.54x$
		87.5	$Cu_{1.0}(In_{0.98}Ga_{0.02})Se_{2.0}$	5.78(3)	11.62(3)	
		100	$Cu_{1.0}(In_{0.97}Ga_{0.03})Se_{2.0}$	5.78(2)	11.61(2)	
gallium content	1.0 Cu + (0.7 In + 0.3 Ga) + 2.0 Se	12.5	$Cu_{1.0}(In_{0.71}Ga_{0.29})Se_{2.0}$	5.73(4)	11.47(4)	
	1.0 Cu + (0.5 In + 0.5 Ga) + 2.0 Se		$Cu_{1.0}(In_{0.51}Ga_{0.51})Se_{1.9}$	5.68(1)	11.37(1)	$a = 5.77 - 0.18x$
	1.0 Cu + (0.3 In + 0.7 Ga) + 2.0 Se		$Cu_{1.0}(In_{0.30}Ga_{0.79})Se_{1.8} + Cu_{2-x}Se$	5.64(2)	11.26(2)	$c = 11.63 - 0.57x$
	1.0 Cu + (1.0 Ga) + 2.0 Se		$Cu_{1.0}(Ga_{1.1})Se_{2.0} + Cu_{2-x}Se$	5.60(2)	11.04(2)	

[a] The lattice parameters were calculated by least-square refinements.

tures, according to the synthetic conditions, for which dissolution of selenium at a high temperature produced the hexagonal structure.[19] Dissolution of selenium at 110 °C by ultrasound treatment produced cubic-phase InSe. This is similar to the controlled growth of cubic InSe nanocrystals by varying the oleylamine concentration, which indicates that the local high temperature caused by ultrasonic cavitation may have induced temporary dissolution of selenium in the hydrazine solution. In addition, the present sonochemical method is more efficient than the solvothermal preparation of InSe at 180 °C.[20]

The $(In_{0.68}Ga_{0.32})Se_{1.81}$ (In-Ga-Se) powder showed an XRD pattern that was similar to that of the $In_{1.00}Se_{1.86}$ precursor, indexed as the cubic or tetragonal structure[21,22] because of the broad peak near $2\theta = 44°$. The sonochemical synthesis incorporated gallium in the pristine InSe lattice and randomly distributed indium and gallium in the metal sites. The final product, $Cu_{1.00}(In_{0.68}Ga_{0.30})Se_{2.01}$, also exhibited approximately 90% yield on the basis of the metals and a smaller cubic cell [$a =$ 5.644(4) Å] than $In_{1.00}Se_{1.86}$. Upon incorporation of Cu^+ and Ga^{3+} cations, which have smaller ionic radii than In^{3+} (Cu^+: 91 pm, Ga^{3+}: 76 pm, In^{3+}: 94 pm), into the zincblende In-Se lattice, the bond length between the cation and anion decreased and the unit cell shrank.[23] The Raman spectra of In-Se, In-Ga-Se, and Cu-In-Ga-Se powder are broad in the Raman shift range of 140 to 250 cm^{-1}, and this was attributed to the TO and LO modes of the zincblende structure (Figure S4).[24]

Figure 5 a–d shows the SEM, TEM, and selected area electron diffraction (SAED) images of the as-synthesized CIGSe nanoparticles by using the sonochemical method in a 12.5% hydrazine solution. The CIGSe nanoparticles possess irregular and pseudospherical shapes and broad size distributions of approximately 50 nm. The HRTEM image demonstrates the agglomeration of 5 nm nanocrystals, the boundary of which corresponds to crystal sizes of 4.1 nm, as estimated by Scherrer's equation from the XRD patterns in Figure 4 c. The inorganic nanocrystals prepared by sonochemical synthesis underwent easy aggregation because of the high surface energy resulting from the absence of organic capping agents.[25,26] The magnified HRTEM image shows the basal spacing of the (111) plane of the cubic zincblende structure, and the SAED image exhibits the polycrystalline ring pattern, probably because the particle size is smaller than the e-beam spot of 100 nm.[27] The (111), (220), and (311) basal spacing values calculated from Figure 5 d are 3.30, 2.06, and 1.73 Å, which is in good agreement with the spacings of the XRD peaks in Figure 4 c.

Figure 5 e–h presents the morphology of CIGSe after annealing at 500 °C under an Ar atmosphere, which resulted in the formation of large crystal grains 100–250 nm in size with well-developed crystal planes. The HRTEM images show lattice fringes that are well-matched to their XRD patterns; the *d* values of 0.202 and 0.332 nm are indicated by white lines in Figure 5 f, g, and they correspond to the {(220), (204)} and (112) peaks, respectively.[28] The SAED patterns indicate that the nanocrystal size of the annealed CIGSe was large enough to have Bragg reflections, for which the zone axis pattern was determined to be [220], as indexed with the chalcopyrite tetragonal structure. The strong reflections of (112), (220), (004), and (116) were observed at 3.38, 2.09, 2.96, and 1.79 Å, respectively.

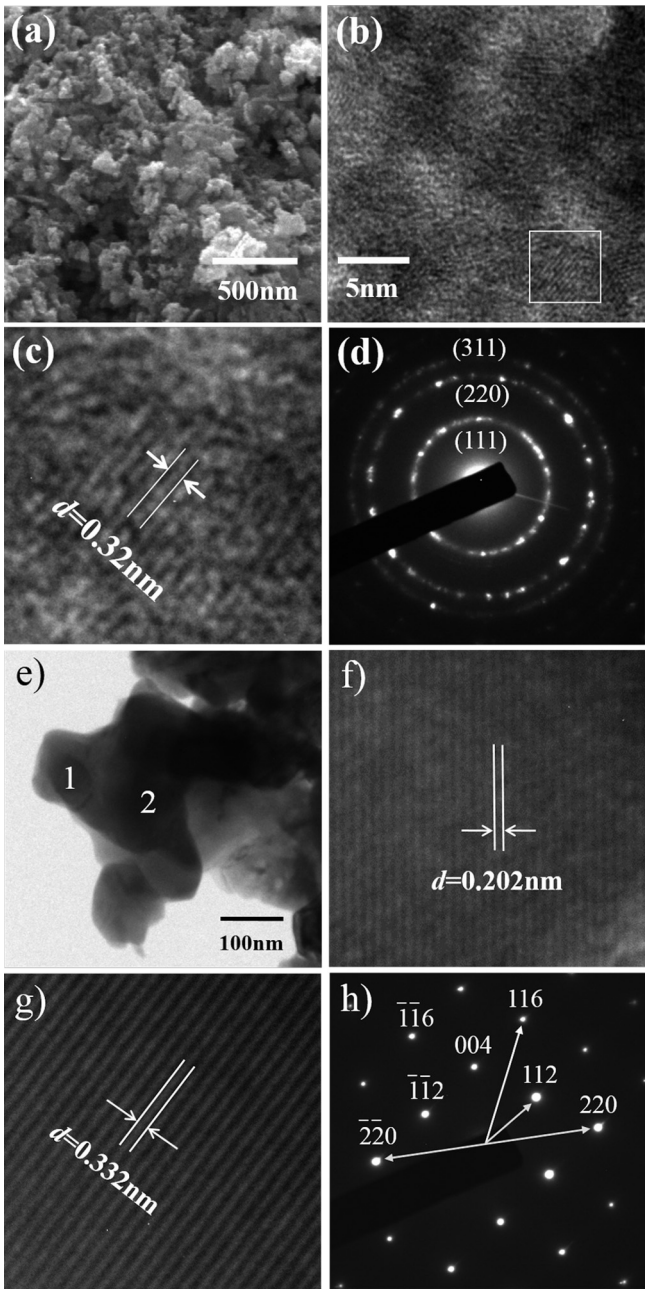

Figure 5. (a) SEM, (b, c) HRTEM, and (d) SAED pattern images of the as-synthesized CIGSe nanoparticles [(c) shows magnified image of (b)]. (e–g) HRTEM and (h) SAED pattern images of the CIGSe nanoparticles annealed at 500 °C; (f, g) are high-resolution images of areas 1 and 2 in (e).

The angles between the (112) and (220) planes and the (220) and (116) planes were 35.7 and 65.2°, respectively, which deviate from 35.3 and 64.8° of the cubic structure; this is indicative of lattice distortion from metal ordering of the tetragonal chalcopyrite structure.[23]

The XRD data of the CIGSe nanocrystal annealed at 500 °C, as shown in Figure 6 a, were assigned to the tetragonal chalcopyrite structure. The lattice parameters by least-squares refine-

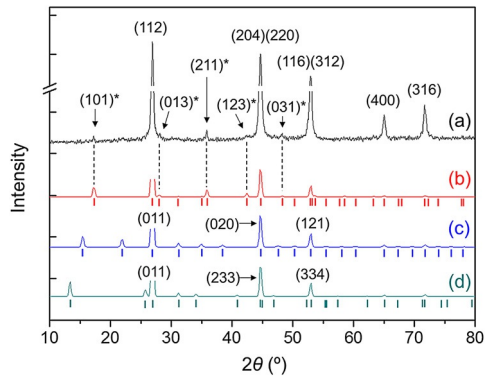

Figure 6. Comparison of the experimental (a) and simulated (b–d) XRD patterns of CIGSe compounds; (b) chalcopyrite, (c) CuAu, and (d) CuPt patterns were simulated by the Atoms program and vertical lines represent the characteristic Bragg's reflection related to each crystal structures.

ments were $a = 5.732(4)$ Å and $c = 11.464(4)$ Å with a tetragonal distortion factor ($c/2a$) of 0.998(4), which agrees with the JCPDS 35-1102 data ($a = 5.736$ Å, $c = 11.448$ Å, and $c/2a = 0.997$). The crystal structures of A(I)B(III)Se_2 compounds derived from the cubic zincblende unit cells are dependent upon the metal sublattice, as shown in Figure 7. The selenium anions (red spheres) occupy the sublattice of the cubic zincblende

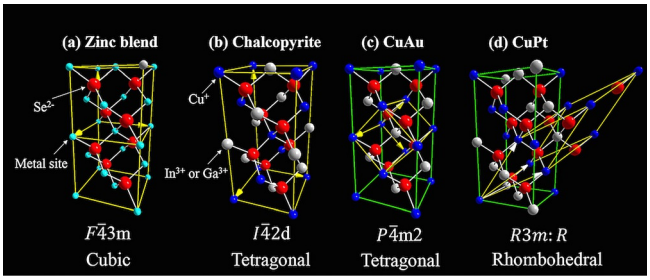

Figure 7. Crystal structures and space groups of (a) zincblende, (b) chalcopyrite, (c) CuAu, and (d) CuPt materials. The yellow arrows are unit cell axes.

structure, but metals can exhibit several behaviors with regard to the order following the Grimm–Sommerfeld rule.[29,30] If A(I)(Cu^+) and B(III)(In^{3+} and Ga^{3+}) are randomly distributed in metal sites (cyan spheres), the unit cell has a zincblende, cubic structure of $F\bar{4}3m$.[29] The ordered occupation of metals could result in tetragonal or rhombohedral structures with three crystal structures: chalcopyrite, CuAu-type, and CuPt-type. The chalcopyrite structure has a specific metal ordering and produces a tetragonal unit cell (I-42d), in which Cu^+ (blue sphere) occupies the (0,0,0) site and In^{3+}/Ga^{3+} (gray sphere) occupy the (1/2,1/2,0) site in metal sublattices.[29] The CuAu-type structure has a tetragonal unit cell of $P\bar{4}m2$, in which Cu^+ is on the (100) plane and In^{3+}/Ga^{3+} is on the (200) plane.[30] The CuPt-type has a rhombohedral cell with $R3m$, in which the Cu^+ and In^{3+}/Ga^{3+} atoms form alternating planes along the [112] direction.[30] The different metal orderings in the lattice induce differences in the direct bandgap energy. In $CuInSe_2$, the CuAu-type and CuPt-type have energies that are smaller than the energy the chalcopyrite structure by 32 and 16 meV, respectively. The first three main XRD peaks observed at $2\theta = 27$, 44, and 53° are common to the three structure types. For example, the peak at $2\theta = 44.6°$ could be indexed as (220) for chalcopyrite, (020) for CuAu-type, and (233) for CuPt-type. The characteristic XRD peaks of the structural simulation were distinguished from the experimental data. For instance, the peaks at $2\theta = 17.26$, 28.05, 35.86, 42.40, and 48.28° corresponding to the (101), (013), (211), (123), and (031) peaks, respectively, are unique to the chalcopyrite structure. The CuAu phase can coexist with chalcopyrite $CuInSe_2$ because of their similar formation energies, but is less likely to occur in chalcopyrite $CuGaSe_2$.[30] Pure chalcopyrite CIGSe may be obtained by incorporating a minimum quantity of Ga into the $CuInSe_2$ precursor.

The Raman spectrum of CIGSe annealed at 500 °C showed a band at a Raman shift of 178 cm^{-1}, the characteristic A_1 vibration mode resulting from the chalcopyrite structure (Figure S4).[31] The Raman spectrum excludes the $Cu_{2-x}Se$ phases generally observed at 260 cm^{-1}, an order vacancy compound (OVC) at 150 cm^{-1}, and the CuAu-type phase at 183 cm^{-1}. The broad band at a Raman shift of approximately 230 cm^{-1} in the as-prepared CIGSe nanocrystals is related to elemental selenium.[32] The Raman spectrum demonstrates that large chalcopyrite-phase CIGSe nanocrystals were obtained by annealing at 500 °C under an inert atmosphere without an additional selenization process to provide selenium sources (Se and H_2Se).

A selected SEM image of the photovoltaic device with glass/Mo/CIGSe/CdS/i-ZnO/AZO/Ni:Al is shown in Figure 8. The

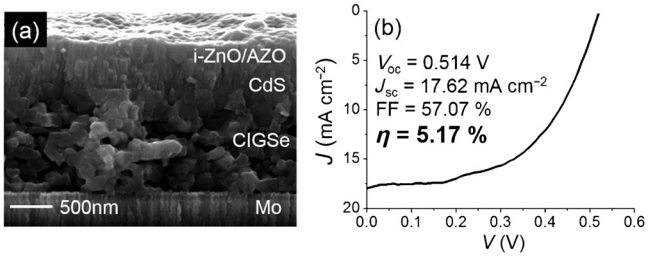

Figure 8. (a) Cross-sectional SEM image and (b) *J–V* characteristics of the solution-processed CIGSe thin-film solar cell.

CIGSe absorber layer with a thickness of 1.2 μm was obtained by annealing in a rapid thermal furnace under an Ar atmosphere at 500 °C for 60 min. The current density–voltage (*J–V*) curve of the prepared device exhibited an efficiency (η) of 5.17% for illumination with a solar simulator of 100 mW cm^{-2}, open-circuit voltage (V_{OC}) of 0.514 V, short-circuit current density (J_{SC}) of 17.62 mA cm^{-2}, and fill factor (FF) of 57% on an active area of 0.44 cm^2. The thin MoSe interfacial layer was beneficial for an increase in ohmic contact between CIGSe and the Mo layer and reduced the series resistance, which resulted in a higher efficiency than that given in the previous report but a similar short-circuit current density.[15]

Conclusions

The synthetic strategy of the sequential addition of metal precursors to a selenium/hydrazine solution to form metal–selenium intermediates was successful and did not include phase separation or formation of amorphous phases. We investigated the correlation between the hydrazine concentration and the composition of gallium in the Cu(In,Ga)Se_2 (CIGSe) nanocrystals and identified a 12.5% hydrazine concentration for $Cu(In_{0.7}Ga_{0.3})Se_2$ to produce an excess amount of hydrazine induced absence of gallium in the CIGSe nanoparticles. The gallium ratios [Ga/(In + Ga)] in CIGSe strongly affected the XRD patterns and the Raman spectra, which enabled the gallium content of the CIGSe samples to be estimated. The as-prepared CIGSe nanoparticles showed a zincblende structure owing to the application of high-energy cavitation, and they were transformed into the chalcopyrite structure by annealing at 500 °C. The chalcopyrite structure of CIGSe was successfully synthesized, and other structure types of metal ordering, such as CuAu- and CuPt-type structures, were excluded. The photovoltaic device, of which the absorber layer was deposited by CIGSe nanoinks, exhibited a solar conversion efficiency of 5.17%. Bandgap tuning of the absorber layer by varying the Ga ratio illustrated the potential of these materials to be promising precursors for highly efficient solution-based CIGSe thin-film solar cells.

Experimental Section

Synthesis of Cu(In,Ga)Se_2 nanoparticles

Copper chloride (CuCl, Junsei, 99.0%), indium acetate [$In(OAc)_3$, Aldrich, 99.99%], gallium nitrate hydrate [$Ga(NO_3)_3 \cdot x H_2O$, Kojundo, 99.99%], selenium (Se, Aldrich, 99.99%), ethylene glycol (Aldrich, 99.8%), and hydrazine monohydrate (Alfa-Aesar, 99%) were used as received without further purification. The precursors were employed in appropriate ratios as described in Table 1. Elemental selenium was dissolved in hydrazine monohydrate, which produced a reddish-brown colloidal solution. After the addition of ethylene glycol and indium(III) acetate, the solution was heated at 110 °C under high-power ultrasonic treatment under an ambient atmosphere for 2 h; the solution changed to a yellow suspension. Gallium(III) nitrate and copper(I) chloride were subsequently added to the mixture, which was treated under ultrasound for 1 h, and a black precipitate was obtained as the final CIGSe product. The CIGSe nanocrystals were separated from the hydrazine/alcohol media by centrifuging at 13000 rpm for 10 min, and the colorless supernatant was decanted. The CIGSe dark powder was washed with deionized water and centrifuged at 10000 rpm for 30 min. Additional washing was performed with ethanol, and the powder sample was dried under vacuum at room temperature. The yield of the prepared CIGSe nanoparticles was approximately 95% on the basis of the amount of copper. The In-Se and In-Ga-Se precursors obtained between subsequent mixing steps were separated, washed, and dried by using a method similar to that described above. Annealing of the CIGSe nanocrystals was performed in a rapid thermal annealing furnace at 500 °C for 1 h under Ar gas flow.

Electron microscopic characterization and spectroscopic analyses

The nanoparticles were characterized by transmission electron microscopy (TEM), scanning electron microscopy (SEM), X-ray fluorescence spectroscopy (XRF), powder X-ray diffraction (XRD) UV/Vis–near-IR spectroscopy, and Raman spectroscopy. TEM images were collected with a JEOL 300 KV instrument operating at 10 kV by drop casting of hexane dispersion of the CIGSe nanoparticles on carbon-coated 200 mesh nickel grids. High-resolution images and selected area electron diffraction (SAED) patterns were obtained at an accelerating voltage of 300 kV. SEM images for CIGSe loaded on a silicon wafer were obtained by using a Philips XL30 ESEM-FEG operating between 10 and 15 keV. The crystal structures of CIGSe and various precursors were characterized by XRD and Raman spectroscopy. XRD patterns of the powder sample were measured with a Rigaku X-ray diffractometer, Ultima IV, in the θ–2θ scanning mode at 40 kV and 30 mA by using CuK_α radiation ($\lambda = 1.5405$ Å). Raman spectra were recorded in backscattering geometry with JY labRam HR fitted with a liquid nitrogen cooled CCD detector. The spectra were collected under ambient conditions by using the 514.5 nm line of an argon-ion laser. Diffuse reflectance spectra were obtained with a Shimadzu UV-3600 UV/Vis–near-IR spectrophotometer by using an ISR-3100 integrating sphere and barium sulfate as a standard. The chemical compositions of the CIGSe nanoparticles were measured by using an XRF spectrometer of a Rigaku WD-XRF ZSX primus II.

Thin-film deposition and solar cell fabrication

A large quantity of CIGSe nanoparticles with a composition of $Cu(In_{0.7}Ga_{0.3})Se_2$ (> 200 g) was synthesized for the solution process of the CIGSe absorber layer. The nanoink CIGSe solutions were prepared by dispersing the freshly prepared CIGSe nanoparticles in hydrazine hydrate. Selenium powder was added to the CIGSe nanoink solution to enable the formation of uniform CIGSe films, to promote proper grain size, and to compensate for the loss of selenium during annealing at 500 °C. The nanoink solution consisted of CIGSe (1.0 g, 15% wt) and selenium (0.02 g, 0.003% wt) in hydrazine hydrate (5.65 g). Spin coating of the CIGSe/hydrazine solution was performed on a 1 μm-thick, Mo-coated soda-lime glass, which was spun at 1000 rpm for 60 s. Owing to the highly toxic and potentially explosive nature of hydrazine, spin coating should be performed in an argon-filled glove box with the oxygen level maintained below a volume of 0.1%. The films were dried for 3 min at 210 °C to evaporate the ink solvents and to form an adhesive CIGSe layer on the Mo substrates. Ten coating cycles were required to fabricate a film with approximately 1 μm thick CIGSe, followed by heat treatment at 525 °C in an argon-filled graphite box for 1 h. The photovoltaic cells were fabricated by a conventional CIGSe cell structure of Mo/CIGSe/CdS/i-ZnO/AZO/Al.

Acknowledgements

This work was supported by the Basic Science Research Program (NRF-2009-0083540), the Technology Development Program for New and Renewable Energies (KETEP-2009-3021010030), and the National Agenda Project Program of Korea Research Council of Fundamental Science and Technology (2N36870-13-164, KRCF).

Keywords: copper · hydrazine hydrate · metal selenides · nanoparticles · thin films

[1] S. E. Habas, H. A. S. Platt, M. F. A. M. van Hest, D. S. Ginley, *Chem. Rev.* **2010**, *110*, 6571 – 6594.
[2] C. J. Hibberd, E. Chassaing, W. Liu, D. B. Mitzi, D. Lincot, A. N. Tiwari, *Prog. Photovoltaics* **2010**, *18*, 434 – 452.
[3] B. Bob, B. Lei, C.-H. Chung, W. Yang, W.-C. Hsu, H.-S. Duan, W. W.-J. Hou, S.-H. Li, Y. Yang, *Adv. Energy Mater.* **2012**, *2*, 504 – 522.
[4] Q. Guo, G. M. Ford, R. Agrawal, H. W. Hillhouse, *Prog. Photovoltaics* **2013**, *21*, 64 – 71.
[5] W. Guo, B. Liu, *ACS Appl. Mater. Interfaces* **2012**, *4*, 7036 – 7042.
[6] C. J. Stolle, M. G. Panthani, T. B. Harvey, V. A. Akhavan, B. A. Korgel, *ACS Appl. Mater. Interfaces* **2012**, *4*, 2757 – 2761.
[7] M. G. Panthani, V. Akhavan, B. Goodfellow, J. P. Schmidtke, L. Dunn, A. Dodabalapur, P. F. Barbara, B. A. Korgel, *J. Am. Chem. Soc.* **2008**, *130*, 16770 – 16777.
[8] S. J. Park, J. W. Cho, J. K. Lee, K. Shin, J.-H. Kim, B. K. Min, *Prog. Photovoltaics* **2014**, *22*, 122 – 128.
[9] S. Jeong, B.-S. Lee, S. Ahn, K. Yoon, Y.-H. Seo, Y. Choi, B.-H. Ryu, *Energy Environ. Sci.* **2012**, *5*, 7539 – 7542.
[10] J. Chang, J. H. Lee, J.-H. Cha, D.-Y. Jung, G. Choi, G. Kim, *Thin Solid Films* **2011**, *519*, 2176 – 2180.
[11] Y. S. Lee, J.-H. Cha, B. K. Min, D.-Y. Jung, *Sol. Energy Mater. Sol. Cells* **2014**, *125*, 138 – 144.
[12] Y. S. Lim, J. Jeong, J. Y. Kim, M. J. Ko, H. Kim, B. Kim, U. Jeong, D.-K. Lee, *J. Phys. Chem. C* **2013**, *117*, 11930 – 11940.
[13] P. Jackson, D. Hariskos, E. Lotter, S. Paetel, R. Wuerz, R. Menner, W. Wischmann, M. Powalla, *Prog. Photovoltaics* **2011**, *19*, 894 – 897.
[14] I. Repins, M. A. Contreras, B. Egaas, C. DeHart, J. Scharf, C. L. Perkins, B. To, R. Noufi, *Prog. Photovoltaics* **2008**, *16*, 235 – 239.
[15] J. H. Lee, J. Chang, J.-H. Cha, Y. Lee, J.-E. Han, D.-Y. Jung, E. C. Choi, B. Hong, *Eur. J. Inorg. Chem.* **2011**, 647 – 651.
[16] Y. Jin, K. Tang, C. An, L. Huang, *J. Cryst. Growth* **2003**, *253*, 429 – 434.
[17] J. Chang, D.-Y. Jung, J. E. Han, *Bull. Korean Chem. Soc.* **2011**, *32*, 434 – 438.
[18] S. Roy, P. Guha, S. N. Kundu, H. Hanzawa, S. Chaudhuri, A. K. Pal, *Mater. Chem. Phys.* **2002**, *73*, 24 – 30.
[19] K. H. Park, K. Jang, S. Kim, H. J. Kim, S. U. Son, *J. Am. Chem. Soc.* **2006**, *128*, 14780 – 14781.
[20] H.-I. Hsiang, L.-H. Lu, Y.-L. Chang, D. Ray, F.-S. Yen, *J. Am. Ceram. Soc.* **2011**, *94*, 3757 – 3760.
[21] R. H. Al Orainy, *Acta Phys. Pol. A* **2012**, *121*, 666 – 672.
[22] M. Mobarak, *Physica B* **2009**, *404*, 1259 – 1263.
[23] Q. Guo, S. J. Kim, M. Kar, W. N. Shafarman, R. W. Birkmire, E. A. Stach, R. Agrawal, H. W. Hillhouse, *Nano Lett.* **2008**, *8*, 2982 – 2987.
[24] J. Weszka, P. Daniel, A. M. Burian, A. Burian, M. Elechower, A. T. Nguyen, *J. Non-Cryst. Solids* **2003**, *315*, 219 – 222.
[25] H. Xu, B. W. Zeiger, K. S. Suslick, *Chem. Soc. Rev.* **2013**, *42*, 2555.
[26] A. Gedanken, *Ultrason. Sonochem.* **2004**, *11*, 47 – 55.
[27] S. Li, Z. Zhao, Q. Liu, L. Huang, G. Wang, D. Pan, H. Zhang, X. He, *Inorg. Chem.* **2011**, *50*, 11958 – 11964.
[28] J. Álvarez-García, B. Barcones, A. Pérez-Rodríguez, A. Romano-Rodríguez, J. Morante, A. Janotti, S.-H. Wei, R. Scheer, *Phys. Rev. B* **2005**, *71*, 054303.
[29] S. H. Wei, S. B. Zhang, A. Zunger, *Phys. Rev. B* **1999**, *59*, R2478 – R2481.
[30] J. L. Martins, A. Zunger, *J. Mater. Res.* **1986**, *1*, 523 – 526.
[31] W. Witte, R. Kniese, M. Powalla, *Thin Solid Films* **2008**, *517*, 867 – 869.
[32] X. Fontané, V. Izquierdo-Roca, L. Calvo-Barrio, J. Álvarez-García, A. Pérez-Rodríguez, J. R. Morante, W. Witte, *Appl. Phys. Lett.* **2009**, *95*, 121907.

Received: December 27, 2014
Published online on May 8, 2015